Eur. Phys. J. Appl. Phys. (2016) 74: 24603
DOI: 10.1051/epjap/2015150335

THE EUROPEAN PHYSICAL JOURNAL
APPLIED PHYSICS

Regular Article

Improvement of pentathiophene/fullerene planar heterojunction photovoltaic cells by improving the organic films morphology through the anode buffer bilayer*

Zouhair El Jouad[1,2], Linda Cattin[3,a], Francisco Martinez[4], Gloria Neculqueo[4], Guy Louarn[3], Mohammed Addou[2], Padmanabhan Predeep[5], Jayan Manuvel[5], and Jean-Christian Bernède[1]

[1] Université de Nantes, MOLTECH-Anjou, CNRS, UMR 6200, 2 rue de la Houssinière, BP 92208, 44000 Nantes, France
[2] LOPCM, Université Ibn Tofail, Faculté des Sciences, BP 133, 14000 Kenitra, Morocco
[3] Université de Nantes, Institut des Matériaux Jean Rouxel (IMN), CNRS, UMR 6502, 2 rue de la Houssinière, BP 92208, 44000 Nantes, France
[4] Departamento de Ciencia de los Materiales, Facultad de Ciencias Físicas y Matemáticas, Universidad de Chile, 2777 Casilla, Santiago, Chile
[5] Laboratory for Molecular Photonics and Electronics, Department of Physics, National Institute of Technology, 673 601 Calicut, Kerala, India

Received: 3 July 2015 / Received in final form: 24 July 2015 / Accepted: 23 September 2015
Published online: 3 May 2016 –

Abstract. Organic photovoltaic cells (OPVCs) are based on a heterojunction electron donor (ED)/electron acceptor (EA). In the present work, the electron donor which is also the absorber of light is pentathiophene. The typical cells were ITO/HTL/pentathiophene/fullerene/Alq_3/Al with HTL (hole transport layer) = MoO_3, CuI, MoO_3/CuI. After optimisation of the pentathiophene thickness, 70 nm, the highest efficiency, 0.81%, is obtained with the bilayer MoO_3/CuI as HTL. In order to understand these results the pentathiophene films deposited onto the different HTLs were characterized by scanning electron microscopy, atomic force microscopy, X-rays diffraction, optical absorption and electrical characterization. It is shown that CuI improves the conductivity of the pentathiophene layer through the modification of the film structure, while MoO_3 decreases the leakage current. Using the bilayer MoO_3/CuI allows cumulating the advantages of each layer.

1 Introduction

Given the problems due to greenhouse gas emission in the use of fossil fuels, renewable energies have received a great attention during these last years. Photovoltaic energy is one of the most promising. In that field, organic photovoltaic cells are, nowadays, extensively studied because of their specific properties such as lightness, flexibility, large area processing low cost. The hearth of these cells is based on a heterojunction electron donor/electron acceptor (ED/EA). Two organic photovoltaic cell (OPVC) families are encountered, that based on a polymer as electron donor and that using small molecules. The polymeric systems, allow achieving the better power conversion efficiency (η) through the optimization of materials used in bulk heterojunction (BHJ) configuration [1]. However, the complicated purification procedure needed induces low performance reproducibility. On the other hand, small molecules OPVCs are classically based on an organic bilayer sandwiched between two electrodes [2]. One of these electrodes must be transparent and the other must be highly reflexive. The bilayer is a heterojunction, between ED and EA. About the electrodes, while aluminum is often used as reflexive cathode, the transparent conductive anode is usually the indium tin oxide (ITO). Small molecules offer several advantages such as more facile synthesis and purification, inherent monodispersity and high tenability [3]. Moreover, recently, an efficiency of 8.5% was achieved using planar heterojunction (PHJ) with an active hearth which consists of three small molecules organic layers [4]. In that work a thiophene oligomer is used as ED, while the EA layer consists in two phthalocyanine chromophores derivatives.

If the properties of the absorbing layer, which is often the ED layer, are decisive, another important layer is the hole transport layer (HTL), which must allow achieving

[a] e-mail: linda.cattin-guenadez@univ-nantes.fr

* Contribution to the topical issue "Materials for Energy Harvesting, Conversion and Storage (ICOME 2015) – Elected submissions", edited by Jean-Michel Nunzi, Rachid Bennacer and Mohammed El Ganaoui

a high hole collection efficiency [5]. It has been already shown that MoO_3 is a very efficient HTL [6,7]. MoO_3 allows adjusting of the band matching to reduce the barrier at the interface anode/electron donor [8], but it does not modifies the molecular orientation and the organic film structure compared to ITO. However, organic semiconductors, comprising π-conjugated molecules usually possess highly anisotropic properties, such as light absorption and carrier transport, which strongly depend on the molecular orientation of the films [9]. For instance, it was shown that, when the ED is copper phthalocyanine (CuPc), the CuPc molecules orientation changes from perpendicular to the substrate when deposited on MoO_3 (or ITO) to parallel to the substrate when deposited onto CuI [10]. So, in the present work different combinations of these layers are used as HTL.

Otherwise, it is important to keep in mind that the efficiency is only one of the criteria for the commercialization of OPVCs. Other important criteria are the ease to synthesize molecules used and their stability. Syntheses of thiophene derivatives are well known and these materials are usually stable. Here, the absorber of light chosen is the pentathiophene (5T). It is known that oligothiophenes and derivatives are among the most promising organic semiconducting materials because of their good transport properties, as well as their tuneable optical properties [11]. Moreover the properties of 5T are stable. All these advantages justify our choice.

We show that the combination MoO_3/CuI is a very efficient HTL. After a complementary study of the effect of the different HTL (MoO_3, CuI, MoO_3/CuI) on the pentathiophene layers properties, we conclude that CuI improves the conductivity of the pentathiophene layers through the modification of the film structure, while MoO_3 decreases the leakage current. Using the bilayer MoO_3/CuI allows cumulating the advantages of each layer.

2 Experimental

2.1 Solar cells fabrication

For the OPVCs, as heterojunction we employed, as said above, 5T as ED and fullerene (C_{60}) as EA. The exciton blocking layer (EBL) was the aluminum tris(8-hydroxyquinoline) (Alq_3). Alq_3 was chosen because it has been shown that it allows fabricating solar cells with increased lifetimes. Moreover, it has been proven to be a very efficient EBL [12,13].

The standard substrate dimensions were 25 mm $\times$ 25 mm. Since ITO covered the whole glass substrates, some ITO must be removed to obtain the under electrode. A 25 mm $\times$ 17 mm section of each substrate was masked, ITO was then etched using Zn + HCl [14].

After scrubbing with soap, the substrates were rinsed in running deionized water, dried under an argon flow and then loaded into a vacuum chamber (10^{-4} Pa). Then the HTL was deposited under vacuum. Three different HTL configurations were probed, MoO_3, CuI, MoO_3/CuI.

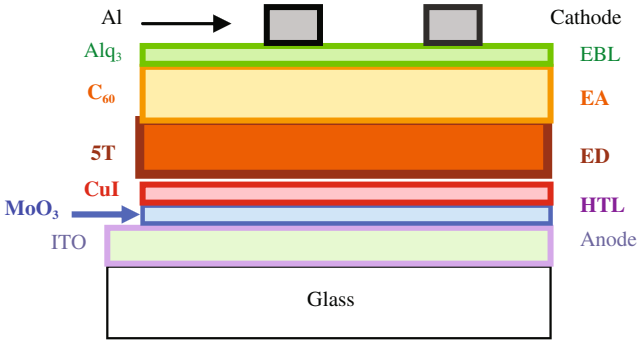

Fig. 1. Schematic representation of an OPVC.

After deposition of the planar heterojunction 5T/C_{60}, the Alq_3 layer and finally the aluminum cathode were deposited. All the films were deposited under a vacuum. The thin film deposition rates and thickness were estimated in situ with a quartz monitor. The deposition rate and the thickness of the MoO_3 layer were 0.02 nm/s and 3 nm respectively [7]. The deposition rate of CuI has a great influence on the properties of the cells [15]. Actually, it is necessary to deposit this film very slowly to prevent current leakage effects. Therefore the CuI film was deposited at a rate of 0.005 nm/s and its thickness was limited at 1.5 nm [16]. The deposition rate for pentathiophene, C_{60} was 0.05 nm/s. The thickness of C_{60} was 40 nm. The thickness of 5T was used as parameter. The deposition rates and thickness of Alq_3 were 0.1 and 9 nm respectively. The fixed thicknesses were chosen after preceding optimizations [14]. After organic thin film deposition, the aluminum top electrodes were thermally evaporated, without breaking the vacuum, through a mask with 2 mm $\times$ 8 mm active areas. In the present work, the effect of the thickness of the 5T film was optimized, then the effect of different HTLs on the OPVCs performance was checked.

The device structures used were: glass/ITO (100 nm)/HTL/5T ($\times$ nm)/C_{60} (40 nm)/Alq_3 (9 nm)/Al(120 nm), with HTL = MoO3 (3 nm), CuI (1.5 nm) or MoO3 (3 nm) CuI (1.5 nm) (Fig. 1).

Chemicals were provided either by Aldrich or by Codex (France). They were used without any purification. Indeed, it has been shown that, using the same charge in the evaporation crucible, there is an "auto purification" of the product during vacuum thin film depositions [17].

2.2 Characterization technique

Electrical characterizations of the OPVCs were performed with an automated I-V tester, in the dark and under global sun AM 1.5 simulated solar illumination. Performances of photovoltaic cells were measured using a calibrated solar simulator (Oriel 300 W) at 100 mW/cm^2 light intensity adjusted with a PV reference cell (0.5 cm^2 CIGS solar cell, calibrated at NREL, USA). Measurements were performed under an ambient atmosphere. All devices were illuminated through transparent conductive electrode (TCO) electrodes. The classical equivalent electrical scheme of OPV cells was used to calculate, the shunt resistance, R_{sh},

Table 1. Photovoltaic performance data of OPVCs using 5T/C_{60} PHJ, with different HTL, under AM1.5 conditions.

HTL	5T thickness (nm)	V_{oc} (V)	J_{sc} (mA/cm^2)	FF (%)	η (%)	R_s (Ω)	R_{sh} (Ω)
MoO_3/CuI	60	0.39	2.54	52	0.52	2.6	850
MoO_3	70	0.40	2.36	59	0.54	4.4	1500
CuI	70	0.30	3.34	34	0.35	4.5	150
MoO_3/CuI	70	0.40	3.64	56	0.81	4.6	1100
MoO_3/CuI	80	0.40	2.43	47	0.45	7	1100
MoO_3/CuI	85	0.41	2.36	44	0.43	12	1150

defined by the slope of the *J-V* curve at $J = J_{sc}$ and the series resistance, R_s, defined by the slope of the *J-V* curve at $J = 0$.

The morphology and layer cross sections were observed through scanning electron microscopy (SEM) with a JEOL 6400F at the "Centre de microcaractérisation de l'Université de Nantes".

AFM images of the films were taken ex-situ at atmospheric pressure and room temperature. All measurements have been performed in intermittent contact mode (Nanosurf Easyscan 2 AFM). The rms roughness given in the following has been calculated by averaging the roughness obtained from each images for a given sample.

The crystalline structure of the films was analyzed by X-ray diffraction (XRD) by a Siemens D8 diffractometer using Kα radiation from Cu ($\lambda = 0.15406$ nm).

Optical absorption spectra were recorded by a Carry spectrophotometer. The optical absorption was measured at wavelengths of 2–0.25 μm.

The highest occupied molecular orbital (HOMO) and lowest unoccupied molecular orbital (LUMO) of pentathiophene were evaluated using cyclic voltammetry. This technique employs a time varying voltage sweep applied to the electrochemical cell containing the material under study, and measurement of resultant current. A three electrodes cell configuration with Pt as the counter electrode is used for this work. The working electrode (here ITO substrate coated with the penthiophene), dipped in an electrolyte solution (acetonitrile containing 0.1 M tetrabutylammonium tetrafluoroborate- $TBABF_4$), is biased with respect to the reference electrode (Ag/AgCl (3 M NaCl)), which has a known potential. A linear ramping potential starting from 0 V up to a pre-defined limiting value with a scan rate of 50 mV/s is applied and resulting current values are recorded. At the optimised limiting potential, the direction of the potential scan is reversed and the current is again recorded. The HOMO and LUMO energy levels are calculated from the following equations [18].

$$\text{HOMO} = \text{Ionization Potential} = -(E_{ox} + 4.4)\ \text{eV}$$
$$\text{LUMO} = \text{Electron Affinity} = -(E_{red} + 4.4)\ \text{eV},$$

where E_{ox} and E_{red} are onset potentials of oxidation and reduction respectively.

3 Experimental results

Since we showed earlier [10,15] that, usually, the HTL bilayer MoO_3 (3 nm)/CuI (1.5 nm) allows achieving the highest OPVCs' efficiencies, we used it for the optimization of the pentathiophene thickness. Then, we checked that MoO_3/CuI is effectively more efficient than MoO_3 or CuI alone.

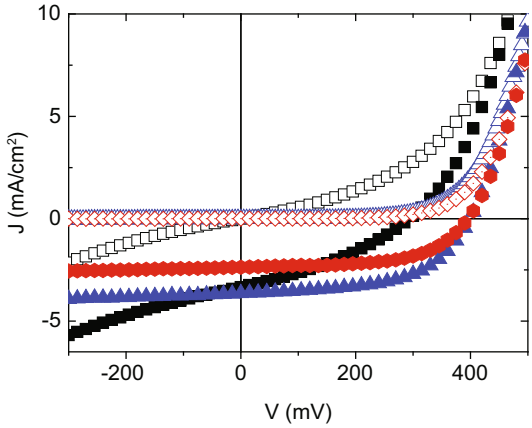

Fig. 2. *J-V* characteristics of OPVCs using 5T as electron donor, and C_{60} as acceptor, with different anode buffer layers: CuI (■), MoO_3/CuI (▲) and MoO_3 (●) in the dark (full symbols) and under AM1.5 irradiation (open symbols).

It can be seen in Table 1 that the optimum thickness of 5T is 70 nm. This optimum thickness is thicker than that usually encountered [19]. A rough estimation of the hole carrier mobility μ_h in the 5T thin films deposited onto MoO_3/CuI using hole only structures (ITO/MoO_3/CuI/5T/MoO_3/Al) gives $\mu_h \approx 1.7 \times 10^{-4}$ cm/V s [20].

Typical *J-V* curves obtained, using the 5T optimal thickness, with different HTL are visualized in Figure 2 and summarized in Table 1. It can be seen that, as expected, the best result is obtained with the double HTL.

The thickness of the 5T film, which was measured with a quartz crystal sensor, was checked by the visualization of the cross section of a 5T film. In Figure 3 we can see the cross section of a 5T film thick of 100 nm, according to the quartz, deposited onto an ITO film thick of 100 nm. It can be concluded that there is a good correlation between the thickness measured by the quartz and that deduced from the cross section visualization. The cross section allows seeing that protrusions are visible at the surface of the 5T layer.

Before a deeper discussion, we proceeded to some more characterizations of the 5T layers.

The LUMO and HOMO values calculated as explained above are 3.37 eV and 5.35 eV respectively. These values

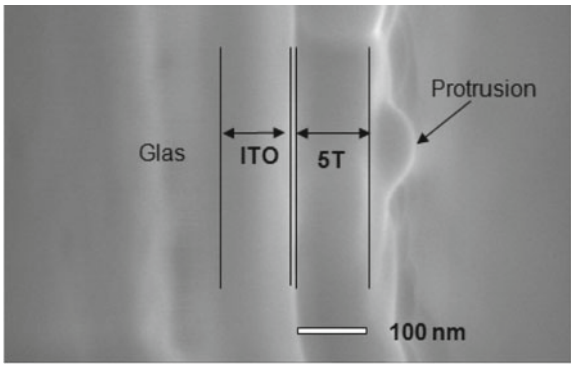

Fig. 3. Visualization of the cross section of 5T film (100 nm) deposited onto ITO/MoO_3/CuI.

confirm that 5T can be a good ED. The potential difference E_g = LUMO-HOMO can be used to estimate the energy gap of the material, it is 1.98 eV.

The optical absorption spectra of 5T film (100 nm thick) are similar whatever the HTL is.

The X-ray diffraction study shows that the structure of the films depends on the HTL. The Figure 4 shows that when the 5T films are deposited onto MoO_3 they are amorphous while diffraction peaks are visible when they are deposited onto CuI. More precisely when the 5T film is deposited onto CuI, the films are at least partly, crystallized, which improves the hole mobility and allows working efficiently with thicker ED layers. As a matter of fact, it has been shown that, if an increase of the carrier mobility improves J_{sc}, it decreases V_{oc}. These two opposite effects balance with one another, resulting in an optimal mobility about 10^{-2} cm^2/V s [21]. In the present work, μ_h is below this optimal value and any μ_h increase will improve the OPVC performances.

The surface visualization by SEM and the AFM images of 5T layers deposited onto different HTL are reported in Figure 5.

Taking into account the difference in scale, we can see that the AFM images of the surfaces are in good agreement with those visualized by SEM. These figures show

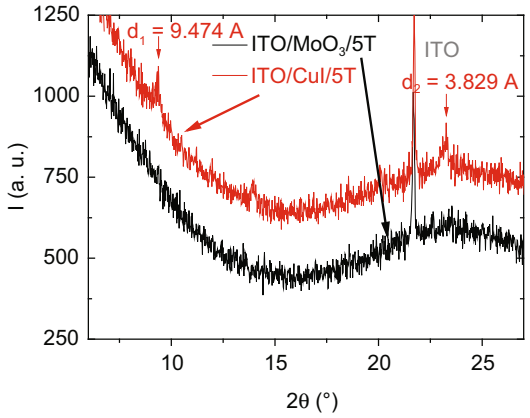

Fig. 4. X-ray diagrams of 5T layers deposited onto MoO_3 and CuI.

significantly different morphologies between the different under-layers.

In Figure 5a, the SEM microphotography of the 5T films deposited onto ITO/CuI exhibits some branches randomly distributed. If the AFM image (Fig. 5d) shows that the 5T film consists in small rod shaped grains, some of these grains are interconnected which gives rise to aggregates in the form of branches such as visualized by the SEM (Figs. 5a and 5d).

In the case of 5T films deposited onto ITO/MoO_3/CuI, the branches are bigger with "crystal shapes" in SEM and AFM images. They are out of the plane of the substrate (Figs. 5b and 5e).

These grains are clearly visible in the cross-section of Figure 3. Conversely, in the case of 5T films deposited onto ITO/MoO_3 they are not branched and the grains, rod shaped and more or less large, are all along the surface of the substrate (Figs. 5c and 5f).

This shows that CuI influence significantly the structure of the 5T films. This fact is corroborated by the X-rays diffraction study.

The characterizations above will now be used to justify the values of the parameters J_{sc}, V_{oc} and FF measured in OPVCs. In the case of 5T/C_{60} planar heterojunctions the optimal values achieved are J_{sc} = 3.64 mA/cm^2, V_{oc} = 0.40 V, FF = 56%, which corresponds to η = 0.81%.

The rms value of 5T films deposited onto MoO_3 is 13.0 ± 0.2 nm, it is 30 ± 2 nm when deposited onto MoO_3/CuI. These values, mainly in the case of MoO_3/CuI are quite high. At first glance, a high roughness of the donor layer allows improving the interface area ED/EA, which has a positive effect on the charge separation and therefore on J_{sc}. In the case of MoO_3/CuI HTL, the heterojunction may be assimilated to a pseudo-bulk-heterojunction, which justifies the better results obtained with this HTL. However such high rms it is not without drawbacks, especially if it rises from the level of the lower electrode. Changes in the morphology of organic films can affect V_{oc}. This might be caused by changes in the local internal field when morphology of material is changed. Indeed, it was shown that too high roughness of the anode has a negative effect on the V_{oc} value due to an increase of the leakage currents [16]. As a matter of fact, the V_{oc} values obtained in this work are quite small. The diagram showing the energy levels of different constituents of the OPVCs is schematized in Figure 6. The maximum theoretical value of V_{oc}, i.e., the energy difference between the LUMO of the acceptor and the HOMO of the donor is 0.85 eV in the case of 5T/C_{60}. The experimental values obtained, 0.4 V, is far smaller. Actually, it can be seen in Table 1 and Figure 2 that V_{oc} depends on the HTL. One can see that, with CuI alone as HTL, the dark current is far higher than that of the OPVCs using MoO_3 as HTL (Fig. 2). Thus, the V_{oc} is consequently enhanced in the OPVCs with MoO_3.

We have already shown that CuI HTL tends to increase the leakage current due to some surface inhomogeneity of the CuI HTL [15,16]. Therefore the best result is achieved with the double HTL MoO_3/CuI. We assume that the reason for this may be the dual function of MoO_3 and

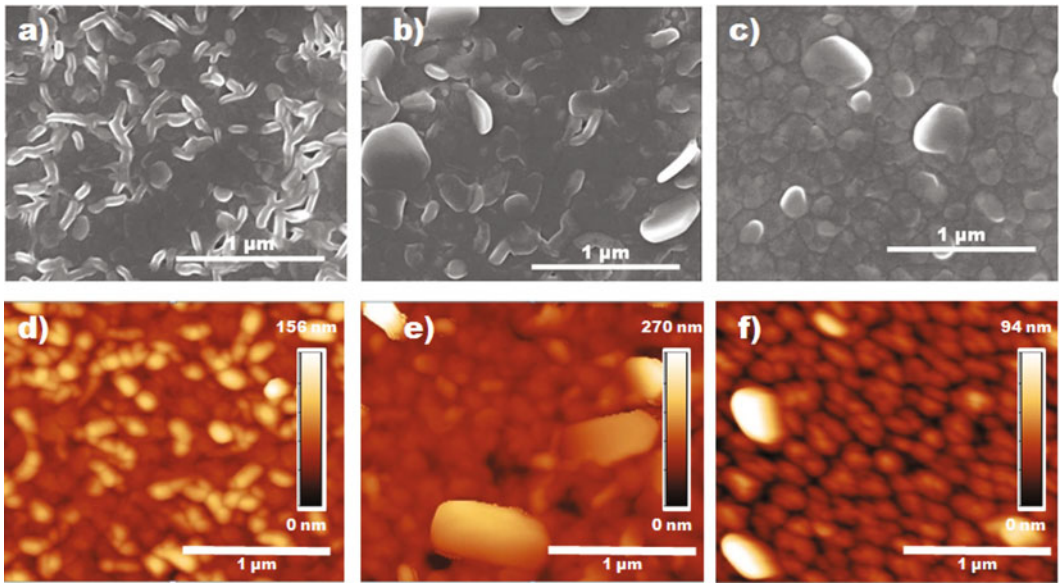

Fig. 5. SEM (a) and AFM (d) images of 5T layer deposited onto ITO/CuI. SEM (b) and AFM (e) images of 5T layer deposited onto ITO/MoO_3/CuI. SEM (c) and AFM (f) images of 5T layer deposited onto ITO/MoO_3.

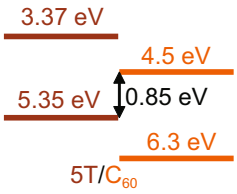

Fig. 6. Schematic band structure of the PHJ 5T/C_{60}.

CuI. CuI improves the crystallinity of the 5T films and increase of the area of the interface ED/EA. For its part, MoO_3 prevents the OPV cells from leakage path formation and allows achieving an optimum band matching between the anode and the HTL.

Another source of decrease of the OPVC performances is the quality of the interface ED/EA [3]. In fact, the V_{oc} value is influenced not only by the energy level difference between the LUMO of the EA and the HOMO of the ED but also by the molecular packing and the charge carrier recombination at the interface [22,23].

4 Conclusion

Even if the absorption of 5T does not match very well the solar spectrum, its crystallinity allows using thick ED films, which permits obtaining significant OPVC efficiency which is improved by the use of double MoO_3/CuI HTL.

This work was financially supported by the Academy Hassan II – PPR/2015/9 (Morocco).

References

1. M.C. Scharber, N.S. Sariciftci, Prog. Polym. Sci. **38**, 1929 (2013)
2. J.C. Bernède, J. Chil. Chem. Soc. **53**, 1549 (2008)
3. Y. Abe, T. Yokoyama, Y. Matsuo, Org. Electr. **14**, 3306 (2013)
4. K. Cnops, B.P. Rand, D. Cheyns, B. Veeet, M.A. Empl, P. Heremans, Nat. Comms. **5**, 3406 (2014)
5. A. Godoy, L. Cattin, L. Toumi, F.R. Diaz, M.A. del Valle, G.M. Soto, B. Kouskoussa, M. Morsli, K. Benchouk, A. Khelil, J.C. Bernède, Sol. Energy Mater. Sol. Cells **94**, 648 (2010)
6. J. Meyer, S. Hamwi, M. Kröger, W. Kowalsky, T. Riedl, A. Kahn, Adv. Mater. **24**, 5408 (2012)
7. J.C. Bernède, L. Cattin, M. Morsli, Technology Letters **1**, 5 (2014)
8. J.C. Bernède, L. Cattin, S. Ouro Djobo, M. Morsli, S.R.B. Kanth, S. Patil, P. Leriche, J. Roncali, A. Godoy, F.R. Diaz, M.A. del Valle, Phys. Status Solidi A **208**, 1989 (2011)
9. H. Peisert, M. Kknupfer, T. Schweiger, J.M. Auerthammer, M.S. Golden, J. Fink, J. Appl. Phys. **91**, 4872 (2002)
10. M. Makha, L. Cattin, S. Dabos-Seignon, E. Arca, J. Velez, N. Stephant, M. Morsli, M. Addou, J.C. Bernède, Indian J. Pure Appl. Phys. **51**, 569 (2013)
11. A. Mishra, P. Bâuerle, Ang. Chem. Int. Ed. **51**, 2020 (2012)
12. Y. Lare, B. Kouskoussa, K. Benchouk, S. Ouro Djobo, L. Cattin, F.R. Diaz, M. Gacitua, T. Abachi, M.A. del Valle, F. Amijo, G.A. East, J.C. Bernède, J. Phys. Chem. Solids **72**, 97 (2011)
13. Q.L. Song, F.Y. Li, H. Yang, H.R. Wu, X.Z. Wang, W. Zhou, J.M. Zhao, X.M. Ding, C.H. Huang, X.Y. Hou, Chem. Phys. Lett. **416**, 42 (2005)
14. Y. Berredjem, N. Karst, L. Cattin, A. Lkhdar-Toumi, A. Godoy, G. Soto, F. Diaz, M.A. Del Valle, M. Morsli, A. Drici, A. Boulmokh, A.H. Gheid, A.H. Gheid, A. Khelil, J.C. Bernède, Dyes Pigm. **78**, 148 (2008)

15. L. Cattin, J.C. Bernède, Y. Lare, S. Dabos-Seignon, N. Stephant, M. Morsli, P.P. Zamora, F.R. Diaz, M.A. del Valle, Phys. Status Solidi A **210**, 802 (2013)
16. M. Makha, L. Cattin, S. Ouro Djobo, N. Stephant, N. Langlois, B. Angleraud, M. Morsli, M. Addou, J.C. Bernède, Eur. Phys. J. Appl. Phys. **60**, 31302 (2012)
17. R.F. Salzman, J. Xue, B.P. Rand, A. Alexander, M.E. Thompson, S.R. Forrest, Org. Electr. **6**, 242 (2005)
18. B.A. Gregg, MRS Bulletin **30**, 20 (2005)
19. J. Sakai, T. Taime, K. Saito, Org. Electr. **9**, 582 (2008)
20. `http://www.npl.co.uk/science-technology/electrochemistry/research/organic-elecronics/mobility-protocol`, 2014
21. J.-T. Shieh, C.-H. Liu, H.-F. Meng, S.-R. Tsebg, Y.-C. Chao, S.-F. Horng, J. Appl. Phys. **107**, 084503 (2010)
22. K. Cnops, B.P. Rand, D. Cheyns, P. Heremans, Appl. Phys. Lett. **101**, 143301 (2012)
23. K. Schulze, C. Uhrich, R. Schüppel, K. Leo, M. Pfeiffer, E. Brier, E. Reinold, P. Bäuerle, Adv. Mater. **18**, 2872 (2006)